Potential Gain in Multicrystalline Silicon Solar Cell Efficiency by n-type Doping

Florian Schindler, Bernhard Michl, Andreas Kleiber, Heiko Steinkemper, Jonas Schön, Wolfram Kwapil, Patricia Krenckel, Stephan Riepe, Wilhelm Warta, and Martin C. Schubert

Abstract— **This work aims for a quantitative investigation of the material limitations and the efficiency potential of an entire multicrystalline (mc) n-type silicon block in comparison to a multicrystalline p-type block of the same purity level in order to predict the potential of mc n-type silicon for the industrial production of solar cells. Therefore, two standard multicrystalline silicon blocks were crystallized under identical conditions (same high purity feedstock, crucible system, and temperature profiles), only differing in their type of doping. The material quality of wafers along the whole block height is analyzed after different solar cell process steps by photoluminescence imaging of the diffusion length. The bulk recombination related efficiency losses are assessed by an "Efficiency limiting bulk recombination analysis" (ELBA) combining injection dependent lifetime images with PC1D cell simulations. The influence of the base resistivity variation along the block is considered in the PC1D cell simulations and backed up by Sentaurus Device simulations. This analysis predicts a significantly higher material-related efficiency potential after typical solar cell processes along the whole block height for mc n-type silicon compared to mc p-type silicon. In addition the efficiency potential for mc n-type silicon depends less on block position.**

Index Terms—**multicrystalline silicon, n-type, iron, resistivity**

I. INTRODUCTION

FOR high efficiency monocrystalline silicon solar cells, n-type silicon is already a proper alternative to p-type silicon and efficiencies beyond 25% have been reached on Cz substrate [1, 2]. N-type silicon features advantages like a smaller impact of certain metal impurities such as interstitial iron on the electrical material quality [3] and the absence of

the boron-oxygen-related degradation [4]. Recent research on multicrystalline (mc) n-type silicon investigated the influence of impurities on the material quality [5-7] and illustrates that mc n-type silicon features high lifetimes [8, 9], large diffusion lengths, and a high efficiency potential after the full solar cell process [10]. Also, the impact of boron and phosphorus diffusion gettering on the edge zone in mc n-type silicon has been investigated [11]. However, a direct comparison of mc n- and p-type silicon crystallized in the same crystallization furnace under identical crystallization conditions has not been performed so far. Predictions of the efficiency potential of state of the art mc n-type silicon compared to mc p-type silicon for a complete block are not available, despite their commercial significance. Such investigations in consideration of the material quality after different solar cell processes and the base resistivity variation along the block height are performed in this work.

In the first part, we introduce the investigated material, the sample processing, and the characterization techniques as well as the performed simulations. In the second part, evaluations of the material quality, the influence of the base resistivity variation, and the efficiency potential combined with a detailed quantification of the efficiency losses are presented. Thus, the origins of the efficiency gain of mc n-type silicon compared to mc p-type silicon can be understood in detail. Finally, we suggest a resistivity optimization for a further efficiency gain in mc n-type silicon.

II. MATERIAL AND METHODS

A. Crystallization and sample processing

For our investigations, a mc n-type silicon block and a mc p-type silicon block, differing only in their type of doping, were crystallized at Fraunhofer ISE. The same high purity feedstock, quartz crucible, and crucible coating is used for the crystallization of both blocks in the same laboratory crystallization furnace adapted for the crystallization of G1 and G2 size silicon blocks. This ensures a comparable impurity distribution in both blocks. Each G2 size block was cut into three bricks, one of which was positioned symmetrically in one half. In this work we focused on 125x125mm² wafers from a brick "A_{middle}" as depicted in Fig. 1 featuring an edge region with limited material quality only at one side. In Fig. 6 and 8, this region of limited material quality is visible at the right edge of the images.

Fig. 1. Photography of one of the investigated blocks. 125x125mm² wafers were cut from the lower central brick ("A$_{middle}$") as depicted by the white frame.

To investigate the material quality along the whole block height, wafers were selected from three block positions, in the following denoted as "bottom", "middle" and "top". Identical block heights were chosen for the n- and the p-type wafers to ensure comparable impurity content in each group of wafers.

Lifetime samples were produced from these wafers: the wafers were subjected to the high temperature steps of three different solar cell processes depicted in Fig. 2, representing a range of current high-efficiency processing development for both doping types. Wafers without any high temperature step from the initial group served as references.

Fig. 2. Sample Processing. The process steps of the group "P-Diff+Firing" (phosphorus diffusion and firing) are representative for a PERC cell concept [12] on p-type substrate, those of the group "B-Diff" (boron diffusion) are typical for a PassDop cell concept with low-temperature metallization [13] on n-type substrate.

The processes included all steps of the corresponding solar cell process except the metallization. This ensures that the material quality of the lifetime samples is identical to the material quality of the final cell and allows for an analysis of the material related efficiency losses. By investigating samples from bottom to top of the blocks we account for all effects like variations in doping and defect distribution. The process steps of the group "P-Diff+Firing" (phosphorus diffusion and firing) are representative for a PERC cell concept [12] on p-type substrate, those of the group "B-Diff" (boron diffusion) are typical for a PassDop cell concept with low-temperature metallization [13] on n-type substrate. In the group "P-Diff" (phosphorus diffusion), the high temperature firing step was left out. By comparing wafers from this group with the material after P-Diff+Firing, we could assess the influence of the firing step on the material quality of mc p- and n-type Si.

B. Characterization Methods

The material quality of each wafer was investigated by means of QSSPL-calibrated photoluminescence imaging (PLI) [14] to obtain images of the minority carrier diffusion length. Although in terms of recombination properties a comparison of excess carrier lifetimes of mc n- and p-type silicon would be the method of choice, we prefer a comparison of the diffusion length, which is the better figure of merit for solar cell efficiencies. By comparing diffusion lengths, the large difference in minority carrier mobility in n- and p-type silicon is accounted for, which allows for a better comparability of the material quality. QSSPL-calibrated PLI was also applied to image the concentration of interstitial iron in the p-type wafers [15]. As discussed before, this also gives access to the interstitial iron concentration in the n-type wafers, as the impurity content should be comparable due to the identical crystallization conditions.

Finally, injection-dependent QSSPL-calibrated PLI allows for an estimation of the solar cell efficiency potential by an "Efficiency limiting bulk recombination analysis" (ELBA) [16] (with the modifications described in [17]): Efficiency maps are calculated based on the injection dependent images of bulk recombination combined with PC1D cell simulations. The efficiency potential is predicted for p-type wafers of the process group "P-Diff + Firing" (a typical PERC cell concept on p-type), and n-type wafers of the group "B-Diff" (a typical PassDop cell concept with low-temperature metallization) and "P-Diff". The choice of these groups will be motivated in detail in section III. C. In this work, the cell concepts used for the simulations were chosen such that the efficiency limit without any bulk recombination ("cell limit") is the same for all concepts and both n- and p-type material. This allows for a direct comparison of the material related efficiency losses. For the n-type samples of the process group "B-Diff", the PassDop concept described in [13] in combination with a Honeycomb texture [18] is used. This leads to an efficiency limit without bulk recombination of 21.8%. The same model was used for the n-type samples of group "P-Diff" to estimate the maximum efficiency limit in the n-type material investigated here. For the p-type samples of the process group "P-Diff+Firing", also a model with a dielectric rear surface passivation [12] with the same optics and the same dark saturation current densities for the front and rear side as in the n-type model ($J_{0,rear} = 45fA/cm^2$, $J_{0,front} = 25fA/cm^2$) is used. This leads to nearly the same efficiency limit without bulk recombination of 21.7%.

The varying base resistivity is accounted for in the PC1D simulations. To support the quality of the predictions from PC1D, independent 3D simulations with Sentaurus Device were performed. N- and p-type PERC structures featuring point contacts and local BSFs on the rear side were investigated for different rear contact pitches. In contrast to the PC1D simulations lateral effects, for example transport of majority carriers to the point contacts at the backside, are accounted for as well. The cell efficiency is predicted for a variation of the bulk lifetime from 1 µs to 10 ms. To determine the influence of the base resistivity, simulations

were performed for $1\,\Omega$cm and $3\,\Omega$cm material, which correspond to the base resistivity extremes in the n-type wafers investigated in this work. Results are presented in section III. A.

III. RESULTS

A. Resistivity variation

Before discussing the recombination properties of the material, we will first focus on the doping variation along the block height. Fig. 3 shows the base resistivity as a function of the block height for the p- and the n-type brick. While the p-type brick features a very homogeneous resistivity along the whole block height due to the segregation coefficient of boron of 0.8, the lower segregation coefficient of phosphorus (0.35) leads to a large variation in the resistivity from higher than $3\,\Omega$cm at the block bottom to lower than $1\,\Omega$cm at the block top of the n-type crystal. As depicted in the graph, wafers were selected from three block positions corresponding to a base resistivity of $1.1\,\Omega$cm (bottom), $1.1\,\Omega$cm (middle), and $0.9\,\Omega$cm (top) in the p-type brick and $2.8\,\Omega$cm (bottom), $2.1\,\Omega$cm (middle), and $1.3\,\Omega$cm (top) in the n-type brick. These values were obtained from inductive measurements on wafer level. Slight deviations compared to Eddy Current measurements on block level plotted in Fig. 3 are attributed to a non-planar crystallization front and changing convection patterns in the silicon melt during crystallization leading to lateral inhomogeneities as well as to uncertainties in the measurement techniques.
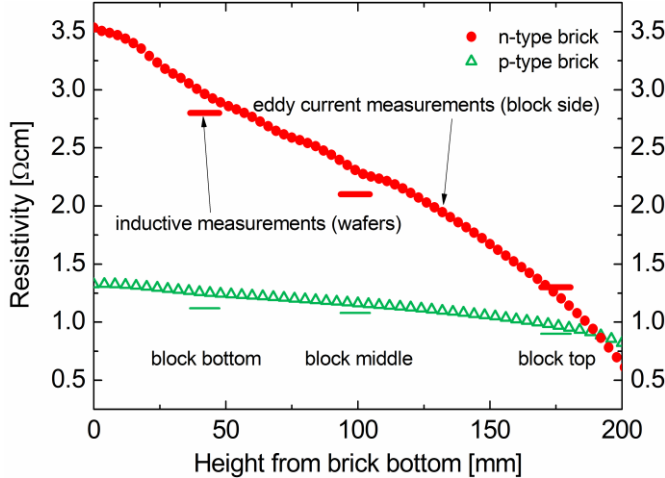

Fig. 3. Resistivity profiles of the n- and p-type bricks along the block height obtained from Eddy Current measurements at the block sides and inductive measurements at wafer level.

As shown in Ref. [19], the base resistivity can have a significant influence on solar cell efficiency. In our paper, a prediction of the efficiency potential is done in section III. C based on a PC1D model. In order to validate the procedure of accounting for the base resistivity variation in the one-dimensional PC1D simulations, the influence of a base resistivity variation on the cell efficiency is compared with 3D simulations using Sentaurus Device as explained in the last section. Fig. 4a) shows the cell efficiency as a function of bulk lifetime simulated with the PC1D cell models used in this

work for n- and p-type silicon with a base resistivity of $1\,\Omega$cm and $3\,\Omega$cm. In both cases, a lower base resistivity leads to higher efficiencies for low to medium bulk lifetimes. For very low bulk recombination, the base resistivity does not significantly influence the cell efficiency any more. As efficiencies are compared as a function of lifetime, the p-type curves are shifted to higher values compared to the n-type curves due to the higher minority carrier mobility.
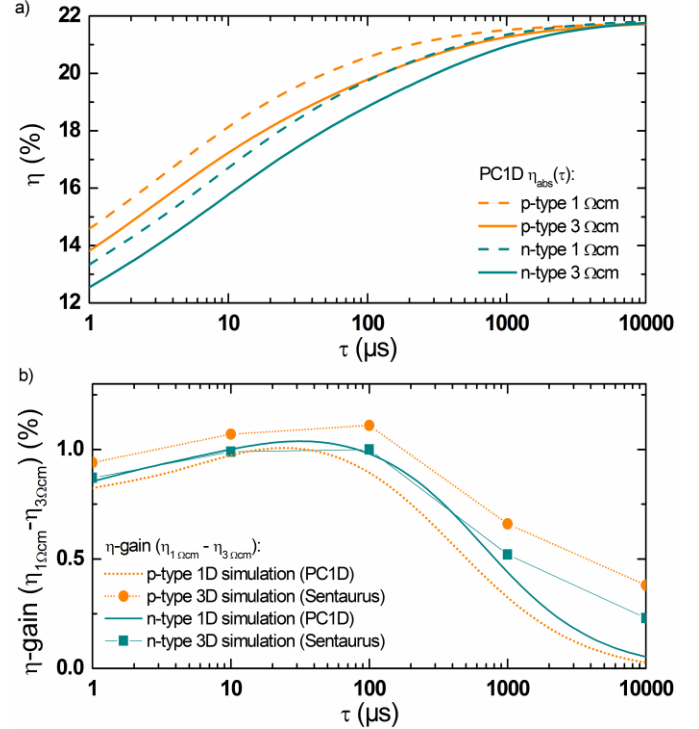

Fig. 4. Impact of base resistivity on the simulated cell efficiency. Graph a) shows the efficiency simulated with the PC1D cell models used in this work as a function of bulk lifetime for n- and p-type silicon with a base resistivity of $1\,\Omega$cm and $3\,\Omega$cm. Graph b) compares the efficiency gain obtained with a $1\,\Omega$cm base compared to a $3\,\Omega$cm base as a function of bulk lifetime simulated with PC1D and Sentaurus Device. Excellent agreement is obtained for n-type silicon up to 1ms.

The Sentaurus Device simulations revealed that the optimum pitch did not depend significantly on the resistivity variation or the lifetime variation. This allows the choice of one pitch regardless of the resistivity or the lifetime leading to maximum differences in the efficiency of less than $0.05\%_{abs}$ compared to the optimum pitch at the specific resistivity and lifetime. Fig. 4b) highlights the efficiency gain obtained with a $1\,\Omega$cm base compared to a $3\,\Omega$cm base as a function of bulk lifetime simulated with Sentaurus Device (3D) (at the optimum pitch of 160 μm for n-type and 320 μm for p-type) and with PC1D. This efficiency gain features a maximum at low to medium bulk lifetime values between 10 μs and 100 μs. For high lifetimes, the base resistivity does not impact the efficiency significantly. Especially for n-type silicon, the PC1D and Sentaurus Device simulations of efficiency gains are in very good agreement. This supports the approach of considering the base resistivity variation in the PC1D cell models for the prediction of the efficiency potential with ELBA applied in this work. The slight deviation at high lifetimes is due to lateral effects (transport of majority carriers

to the point contacts at the backside) which are not accounted for in the 1D simulations with PC1D.

B. Material Quality

In a second step, the material quality after different solar cell process steps is evaluated. Fig. 5 shows the harmonically averaged diffusion length across wafers from three different positions of the n-type block (filled columns) and the p-type block (dashed columns) at a generation rate of 0.05 suns, which is estimated to correspond to an injection level close to MPP-conditions in the solar cell. As mentioned before, comparing the diffusion length in n- and p-type silicon already accounts for the lower minority carrier mobility in n-type, such that this allows for a direct comparison of the material quality of mc n- and p-type silicon.
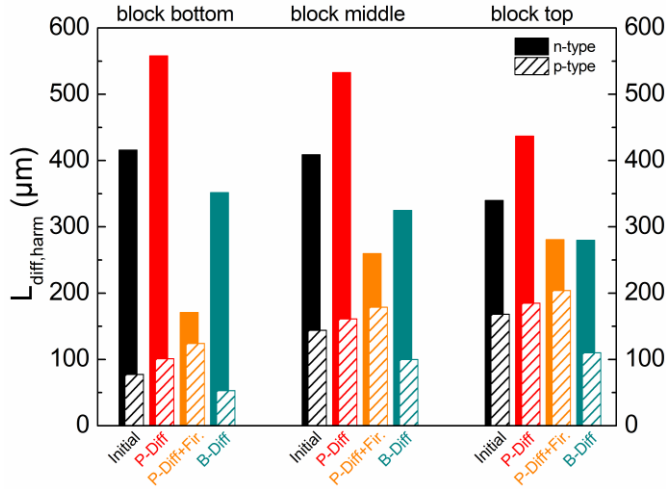

Fig. 5. Harmonically averaged diffusion length across wafers from three different positions of the n-type block (filled columns) and the p-type block (dashed columns) at a generation rate of 0.05 suns, which is estimated to correspond to an injection level close to MPP-conditions in the solar cell. The n-type samples feature significantly higher diffusion lengths along the whole brick after all process steps.

The n-type samples feature significantly higher diffusion lengths along the whole brick after all process steps. Applying a phosphorus diffusion improves the diffusion length in both blocks due to gettering of impurities. Especially in the n-type wafers, the diffusion length is increased significantly (excess carrier lifetimes averaged across the best 1x1cm² exceed 2ms). A subsequent firing step further enhances the diffusion length in p-type silicon, which can be attributed to a hydrogen passivation from the silicon nitride stack [20], while it significantly reduces the diffusion length in the mc n-type wafers. Cooling to room temperature is typically much faster in a firing step compared to doping process in a tube furnace. Thus a possible explanation of the decrease in diffusion length could be initially large precipitates that dissolve and redistribute to a higher density of smaller precipitates or dissolved impurities limiting in n-type silicon. These dissolved impurities could be Co_s, Cr_i or other defects that have comparable or even higher impact on the charge carrier lifetime in n-type. An alternative explanation is the diffusion of formerly gettered impurities from the emitter into the bulk [21, 22]. The boron diffusion degrades the material quality of

both, the n- and p-type wafers, compared to the initial state. However, the diffusion length in n-type is still on a high level ($\geq 300\mu m$; excess carrier lifetimes averaged across the best 1x1cm² exceed 1ms) and much larger than in p-type after any process step. This is of importance, as a standard n-type solar cell process includes a boron diffusion. The material degradation after the boron diffusion is attributed to the higher temperature (890°C) compared to the phosphorus diffusion (800°C) and to the lower gettering efficacy of the boron diffusion. The effectiveness of boron diffusion gettering strongly depends on the process parameters, as discussed in detail in [23]: While an optimized boron diffusion gettering can effectively getter metal impurities such as Fe and thus increase the electrical quality of the bulk material, a standard boron diffusion can be virtually ineffective in terms of gettering at temperatures above 850°C and even harm the material quality due to a potential cross-contamination from the furnace tube at high temperatures, as suggested in [23]. The higher temperatures of a boron diffusion also lead to a stronger dissolution of precipitates compared to a phosphorus diffusion at lower temperatures, which could additionally harm the material quality. Since it is the aim of this work to investigate the influence of high performance cell processes on the material quality of mc silicon, the boron diffusion chosen here was optimized for emitter and solar cell performance and features a rather weak gettering efficacy.

Focusing on the material quality along the block height, we observe a different trend in the n- and p-type block: While the material quality increases towards the top in the p-type brick, it decreases in the n-type brick after most process steps. This can be explained by the different limitations in mc n- and p-type silicon, which can be observed in the diffusion length images. Fig. 6. shows the central stripe of each wafer after each process step from the block bottom to the block top for n-type (left column) and p-type (right column). Blurring in the PL images was reduced by applying a 1000nm short pass filter in addition to the standard set of long pass filters in front of the CCD camera.

The increasing material quality in the p-type wafers towards the block top can be explained as follows: The lowest position is still affected by dissolved impurities diffused into the crystallized block from the crucible bottom by solid-state diffusion, especially iron. This lowers the diffusion length across the whole wafer. Iron imaging revealed a concentration of interstitial iron of $3x10^{11} cm^{-3}$ in the center of the initial wafer from the block bottom, limiting the lifetime in 1.1 Ωcm p-type silicon to 8µs at low level injection. At the medium block height, the concentration of interstitial iron in the center of the initial wafer is one magnitude lower ($2.5x10^{10} cm^{-3}$). Here, only the edge region is limited by a large concentration of interstitial iron of $1x10^{12} cm^{-3}$. The additional increase in the averaged diffusion length from medium block height to the block top can be attributed to the smaller edge region, which has nearly completely disappeared in the wafers from the block top. The edge region is limited by impurities diffused into the crystallized block by solid-state diffusion during the cooling of the block, mainly iron. As the upper part

crystallized later, here the time for in-diffusion and thus the width of the edge region is reduced. As it is mainly dissolved impurities that limit the diffusion length in mc p-type silicon, these effects lead to the observed trends in the material quality along the block height.
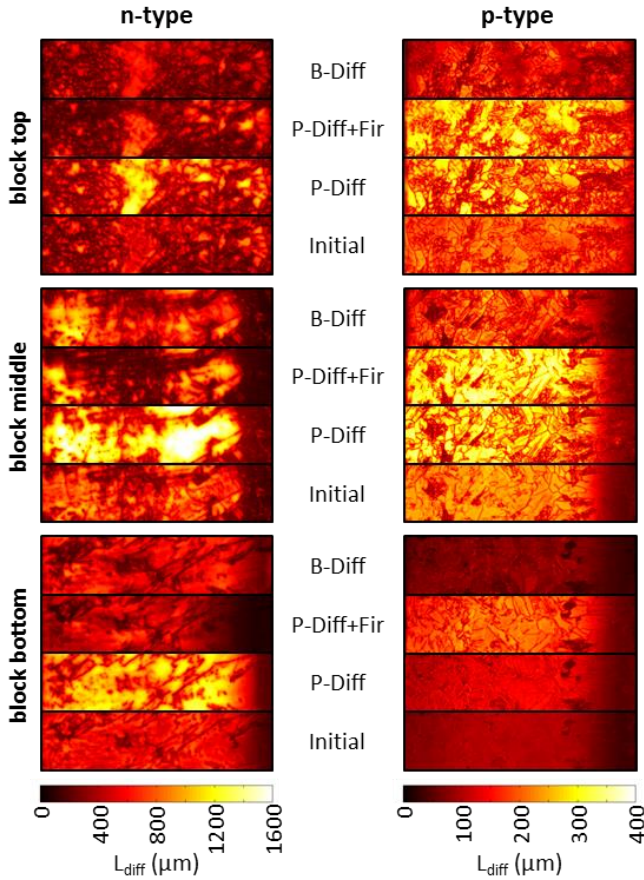

Fig. 6. Diffusion length images. Blurring was reduced by the use of a 1000nm short pass filter. Each image shows the diffusion length of a central stripe (125x31.25 mm²) of the wafers at a generation rate of 0.05 suns after each process step for a certain block position. The impact of the edge region close to the crucible is visible on the right side of the wafers. The left column shows the results on the n-type wafers, the right column on the p-type wafers. Note the factor of four in the scale of the n-type wafers compared to the p-type wafers.

In mc n-type silicon, the recombination properties of impurities are significantly different. We will discuss the effect on the example of interstitial iron. Iron imaging performed on the p-type wafers revealed a maximum concentration of interstitial iron of $3 \times 10^{12} \, cm^{-3}$ in the edge region of initial wafers from the block bottom. Due to the asymmetrical capture cross sections for electrons and holes, lifetime in $1.1 \, \Omega cm$ p-type silicon is limited by this concentration of interstitial iron below 1µs at low level injection, while the limitation in n-type silicon is well above 400 µs. Measured lifetimes in the edge region of an initial n-type wafer from the block bottom are lower than 100 µs, which is why we can exclude a limitation by interstitial iron. However, iron precipitates could contribute significantly to the recombination in the edge region [24]. In the central parts of the wafers, the maximum concentration of interstitial iron was measured to be $3 \times 10^{11} \, cm^{-3}$ before processing in the block

bottom, which limits the lifetime in n-type silicon above 4ms. Therefore, we can also exclude a limitation by interstitial iron in the central parts of the n-type wafers. As visible in the diffusion length images in Fig. 6, it is mainly decorated crystal defects that limit the material quality in mc n-type silicon. As the density of crystal defects, such as grain boundaries and dislocation clusters, increases towards the block top [25], the averaged diffusion length decreases with increasing block height in the n-type brick in the initial state and after the P- and B-diffusion. An exception is observed after firing, which increases the impact of homogeneously distributed impurities and inverts the trend. The diffusion length image of the n-type wafer from the block bottom reveals a significantly larger edge region of low diffusion length after P-diffusion and firing. The reason for this is still unclear and currently under investigation. As mentioned above, it could be attributed to either a redistribution of precipitates or the dissolution of impurities with a comparable or even higher impact on the charge carrier lifetime in n-type.

C. Solar Cell Efficiency Potential

Combining injection dependent bulk lifetime images with PC1D cell simulations as explained in section II. B, the efficiency potential is predicted for p-type wafers of the process group "P-Diff+Firing", and n-type wafers of the group "B-Diff" and "P-Diff". These processing groups have been chosen for the following reasons: As explained in section II. A, the processing conditions from group "P-Diff+Firing" on p-type and "B-Diff" on n-type are representative for typical cell concepts. A comparison of n-type wafers from the group "B-Diff" with p-type wafers from the group "P-Diff+Firing" therefore allows for a fair-minded comparison of the material quality and the efficiency potential of both materials after cell process steps suitable for the production of solar cells on each material. On p-type, the standard processing "P-Diff+Firing" also leads to the best material quality (see section III. B). On the n-type material, the highest diffusion lengths are achieved after P-diffusion, which could be due to a limitation by a metal like chromium, which is also harmful in n-type [26] but can be effectively gettered [27]. Therefore, we also include these samples in the evaluation in order to assess the upper limit of the efficiency potential in this material. However, an advanced cell concept would have to be applied to these samples to realize a solar cell on n-type base material after a P-diffusion without a further B-diffusion and high temperature step. A possibility would be a cell structure with a low temperature emitter (e.g. a hetero structure).

Fig. 7 illustrates the global efficiencies for these three processing groups as a function of block height. In combination with the spatially resolved efficiency maps (c.f. Fig. 8), the pre-characterization of the material quality, and the influence of the base resistivity in sections III. A and B, these results will now be discussed in detail.

The mc p-type wafers feature an efficiency potential between 18% at the block bottom and 19% at the block top. The increase in efficiency towards the block top correlates with the increase in material quality as demonstrated in section

III. B. The variation of the base resistivity is negligible along the p-type brick and does not affect the efficiency potential.
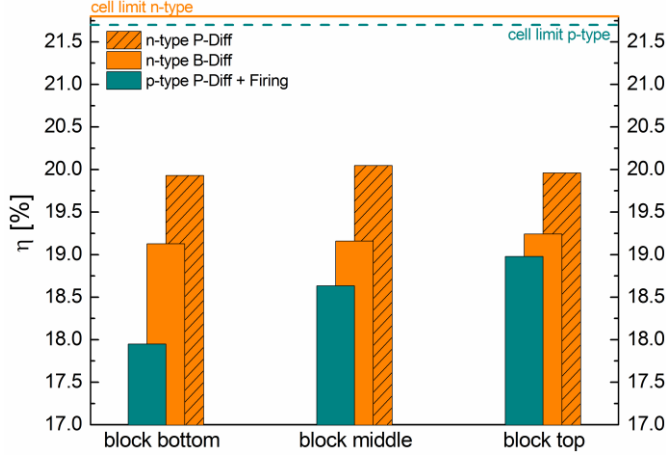

Fig. 7. Efficiency potential as a function of block height for mc p-type after P-diffusion and firing, mc n-type after B-diffusion, and mc n-type after P-diffusion. The efficiency limit (without SRH recombination) of the cell concept is 21.7% for p-type and 21.8 % for n-type.
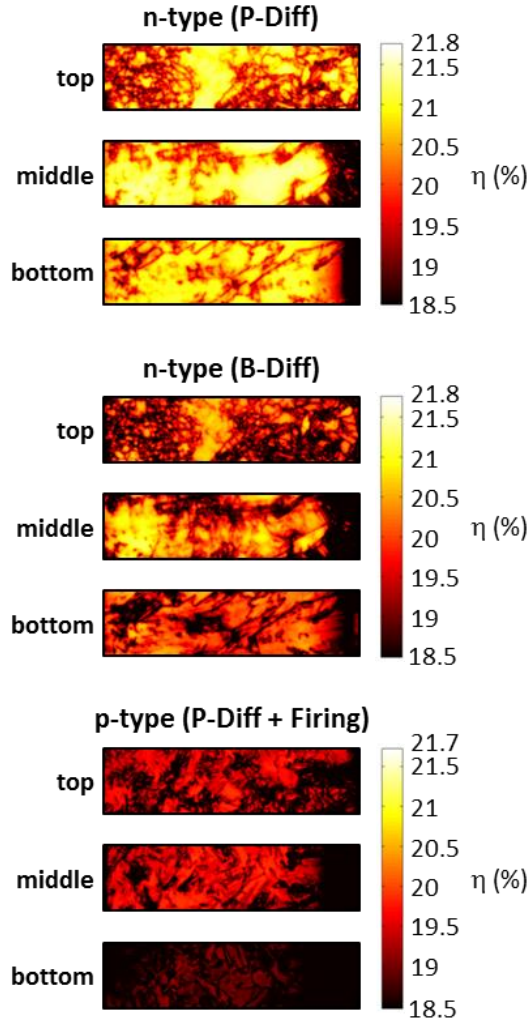

Fig. 8. Spatially resolved efficiency potential of mc p-type after P-Diff+Firing (bottom), mc n-type after B-Diff (middle), and mc n-type after P-Diff (top). The images show the central quarter stripe of wafers from the block bottom, middle and top.

A significant increase in efficiency is observed for the mc n-type wafers after the boron diffusion compared to the p-type wafers: The efficiency potential of these wafers is at a stable level of about 19.2% along the whole block height, which corresponds to an increase averaged along the block height of $+0.7\%_{abs}$ compared to the p-type wafers after P-diffusion and firing. The n-type wafers after a P-diffusion feature the best efficiency potential: A stable level of about 20.0% is reached along the whole block height. Compared to the p-type wafers, this means a considerable gain in efficiency of $+1.5\%_{abs}$ averaged along the brick.

To understand the stable efficiency level of the n-type wafers, we have to go back to the results of sections III. A and B. On the one hand, the material quality of the n-type wafers decreases towards the block top, as explained in section III. B. On the other hand, the base resistivity decreases from 2.8 Ωcm for wafers from the bottom to 1.3 Ωcm for wafers from the top, which leads to an efficiency gain of approximately (0.5-1)$\%_{abs}$ for lifetimes between 1µs and 1ms, as illustrated in Fig. 4. Thus, with increasing block height the decrease in material quality is compensated by a resistivity related efficiency gain, leading to a very stable efficiency level along the whole height of the n-type block.

A spatially resolved analysis (c.f. Fig. 8) shows that while in the p-type sample the efficiency is below 20% also in the best grains, the best 1x1cm² area in the n-type sample "B-Diff" from the medium block height features an efficiency of 21%. In the n-type sample "P-Diff" from the medium block height, the efficiency potential in the best 1x1cm² areas (21.5%) is already close to the cell limit.

D. Efficiency Losses

In a last step, we quantify the efficiency losses and specify their origin in each material. This is done by evaluating the efficiency potential in the best 1x1cm² area virtually free of structural crystal defects. The loss occurring in this region compared to the cell limit can be attributed to homogeneously distributed recombination centers (orange part of the columns in Fig. 9). This comprises dissolved impurities stemming from
(i) the feedstock
(ii) the in-diffusion from the crucible system into the liquid silicon before crystallization and
(iii) the solid-state in-diffusion from the crucible bottom (for the lowest block position)
that remained after processing as well as dissolved impurities additionally incorporated during processing.

The additional recombination loss via crystal defects such as dislocations and grain boundaries (probably) decorated with impurities (cyan dashed part of the columns in Fig. 9) can be assessed by evaluating the efficiency loss in the whole wafer excluding the edge region. Finally, an evaluation of the whole wafer additionally takes into account the losses in the edge region due to impurities diffused into the solid crystal from the crucible walls (grey part of the columns in Fig. 9).
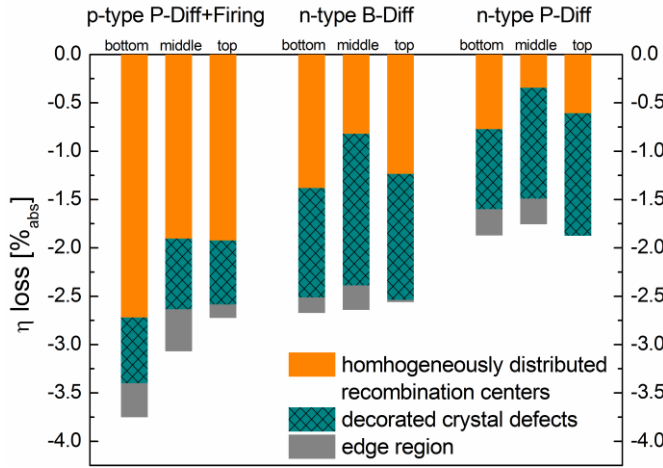
Fig. 9. Efficiency losses in mc p-type after P-Diff+Firing (left), mc n-type after B-Diff (center), and mc n-type after P-Diff (right) for three different block positions (left to right within each group: bottom – middle – top).

The following conclusions can be drawn from this analysis: While in mc p-type silicon dissolved impurities lead to an efficiency loss of $1.9\%_{abs}$ (middle, top) up to $2.7\%_{abs}$ (bottom, see discussion in section III. B) and limit the global efficiency potential, efficiency losses in the n-type samples are mainly due to decorated crystal defects $(-(1.1-1.6)\%_{abs}$. after B-diffusion and $-(0.8-1.3)\%_{abs}$. after P-diffusion). Especially after the P-diffusion, efficiency losses in the good grains of the n-type wafer from medium block height are very low ($-0.3\%_{abs.}$), which leads to an efficiency potential close to the cell limit in these areas. As measured effective lifetimes in these grains exceed 2ms, remaining limitations could even partially be attributed to recombination at the surfaces of the SiN-passivated samples.

As mentioned in section III. C, efficiency losses in the bottom part of the n-type brick are as large as in the top part, despite the larger diffusion length in the bottom part. This is attributed to the higher base resistivity. In a last estimation, we want to discuss the benefit from a lower base resistivity. Besides raising the cell efficiency potential, a lower base resistivity and thus a higher doping concentration also comes along with two disadvantages. First, it leads to a lower minority carrier mobility. This impact, however, is negligible: A base resistivity decrease from $2.8\,\Omega cm$ to $1\,\Omega cm$ is correlated with a decrease of the minority hole mobility of about 4%, leading to a reduction in the diffusion length of about 2%. Second, a higher doping concentration leads to an increased Auger- and SRH-recombination and thus lower charge carrier lifetimes. The efficiency gain obtained by a lower base resistivity is estimated as follows. We fit the measured injection dependent lifetime averaged across the whole wafer (square root harmonic mean) with two fictive defect levels according to the SRH-statistics. This delivers an analytical expression for the injection dependent lifetime at the actual doping concentration. By changing the doping concentration in this expression, we obtain an estimation for the injection dependent lifetime of the same sample at another base resistivity. Now, we read out the generation rate at MPP conditions from the original curve. The new expression for the

injection dependent lifetime delivers the corresponding lifetime value at the same generation rate for the new doping concentration. Thus we take an enhanced recombination at an increased doping concentration into account. It should be mentioned that, as the injection dependent lifetime is simulated with two fictive defect levels, the actual lifetime value at a higher doping concentration could deviate from the simulated value. Still, in our opinion the lifetime obtained from this approach is a better estimate for the real conditions than not taking into account changes in lifetime due to increased recombination at all. Using this lifetime and the new resistivity as input for a PC1D simulation with the models introduced before delivers an estimation for the efficiency potential. As the input is the lifetime value, even the change in minority carrier mobility is taken into account directly by the cell model. We apply this approach to the n-type samples after both B- and P-diffusion, assuming a constant base resistivity of $1\,\Omega cm$ along the whole brick (in reality, this could be achieved by continuous feeding of undoped silicon feedstock during the crystallization process). This allows for a quantification of the efficiency gain due to an optimized base resistivity. Similar to the illustration of losses in Fig. 9, Fig. 10 shows the bulk related efficiency losses for the mc n-type wafers at a virtual base resistivity of $1\,\Omega cm$ and quantifies the additional losses due to the higher actual resistivity.
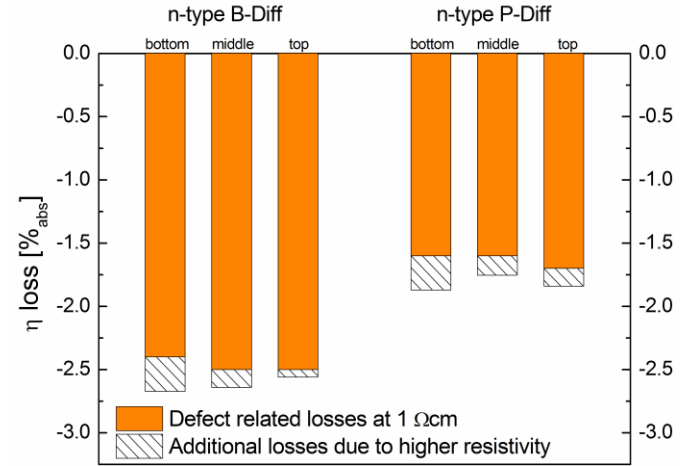

Fig. 10. Efficiency losses as a function of block height for mc n-type after B-diffusion and mc n-type after P-diffusion. The white shaded parts of the columns illustrate the additional efficiency loss due to the actual base resistivity compared to a virtual base resistivity fixed at $1\,\Omega cm$ along the whole brick.

The resistivity-related loss analysis shows, that a shift to lower base resistivity would be beneficial for mc n-type solar cell efficiencies. Thus, the advantage of mc n-type compared to mc p-type silicon is even more obvious comparing both materials at a similar base resistivity.

IV. CONCLUSION

A comprehensive analysis of the efficiency losses after different solar cell processes caused by multicrystalline p- and n-type silicon material along the whole brick highlights the high potential of mc n-type silicon. Compared to a standard solar cell process (P-diffusion + firing) on mc p-type silicon

produced with identical feedstock and under identical crystallization conditions, an average efficiency potential gain of $0.7\%_{abs}$ along the whole block height is found by changing the type of doping and applying a standard solar cell process on n-type (B-diffusion). A huge gain of $1.5\%_{abs}$ in average along the whole block is expected by applying an advanced cell process including solely a P-diffusion to the mc n-type material compared to the mc p-type silicon. We show that the main limitations in mc p-type silicon are dissolved impurities, while mc n-type silicon is limited by decorated crystal defects. Thus, a further gain can be expected by optimizing the crystallization, which suggests a high potential of n-type high performance multicrystalline silicon with a low density of dislocation clusters. An estimation of the influence of the base resistivity on the efficiency potential reveals a benefit from higher doping concentrations.

ACKNOWLEDGMENT

REFERENCES

[1] M. A. Green, K. Emery, Y. Hishikawa, W. Warta, and E. D. Dunlop, "Solar cell efficiency tables (version 44)," *Progress in Photovoltaics: Research and Applications,* vol. 22, pp. 701-710, 2014.

[2] K. Masuko, M. Shigematsu, T. Hashiguchi, D. Fujishima, M. Kai, N. Yoshimura, T. Yamaguchi, Y. Ichihashi, T. Yamanishi, T. Takahama, M. Taguchi, E. Maruyama, and S. Okamoto, "Achievement of more than 25% conversion efficiency with crystalline silicon heterojunction solar cell," in *Proceedings of the 40th IEEE Photovoltaic Specialists Conference*, Denver, Colorado, USA, 2014.

[3] D. Macdonald and L. J. Geerligs, "Recombination activity of interstitial iron and other transition metal point defects in p- and n-type crystalline silicon," *Applied Physics Letters,* vol. 85, pp. 4061-3, 2004.

[4] J. Schmidt, A. G. Aberle, and R. Hezel, "Investigation of carrier lifetime instabilities in Cz-grown silicon," in *Proceedings of the 26th IEEE Photovoltaic Specialists Conference*, Anaheim, California, USA, 1997, pp. 13-18.

[5] J. Libal, "Multikristallines n-Typ Silizium: Materialcharakterisierung und Solarzellenprozessierung," Dissertation, Fachbereich Physik, Universität Konstanz, Konstanz, 2006.

[6] L. J. Geerligs, Y. Komatsu, I. Röver, K. Wambach, I. Yamaga, and T. Saitoh, "Precipitates and hydrogen passivation at crystal defects in n- and p-type multicrystalline silicon," *Journal of Applied Physics,* vol. 102, p. 093702, 2007.

[7] G. Coletti, R. Kvande, V. D. Mihailetchi, L. J. Geerligs, L. Arnberg, and E. J. Øvrelid, "Effect of iron in silicon feedstock on p- and n-type multicrystalline silicon solar cells," *Journal of Applied Physics,* vol. 104, p. 104913, 2008.

[8] A. Cuevas, M. J. Kerr, C. Samundsett, F. Ferrazza, and G. Coletti, "Millisecond minority carrier lifetimes in n-type multicrystalline silicon," *Applied Physics Letters,* vol. 81, pp. 4952-4, 2002.

[9] C. Schmiga, J. Schmidt, M. Ghosh, A. Metz, and R. Hezel, "Gettering and Passivation of Recombination Centres in n-type Multicrystalline Silicon," in *Proceedings of the 19th European Photovoltaic Solar Energy Conference*, Paris, France, 2004, pp. 439-442.

[10] B. Michl, J. Benick, A. Richter, M. Bivour, J. Yong, R. Steeman, M. C. Schubert, and S. W. Glunz, "Excellent average diffusion lengths of 600 µm of n-type multicrystalline silicon wafers after the full solar cell process including boron diffusion," *Energy Procedia,* vol. 33, pp. 41-9, 2013.

[11] V. Vähänissi, M. Yli-Koski, A. Haarahiltunen, H. Talvitie, Y. Bao, and H. Savin, "Significant minority carrier lifetime improvement in red edge zone in n-type multicrystalline silicon," *Solar Energy Materials and Solar Cells,* vol. 114, pp. 54-58, 2013.

[12] P. Engelhart, G. Zimmermann, C. Klenke, J. Wendt, T. Kaden, M. Junghänel, K. Suva, B. Barkenfelt, K. Petter, S. Hermann, S. Schmidt, D. Rychtarik, M. Fischer, J. W. Müller, and P. Wawer, "R&D pilot-line production of multi-crystalline Si solar cells with top efficiencies exceeding 19%," in *Proceedings of the 37th IEEE Photovoltaic Specialists Conference*, Seattle, Washington, USA, 2011, pp. 1919-23.

[13] D. Suwito, U. Jäger, J. Benick, S. Janz, M. Hermle, and S. W. Glunz "Industrially feasible rear passivation and contacting scheme for high-efficiency n-type solar cells yielding a V_{oc} of 700 mV," *IEEE Transactions on Electron Devices,* vol. 57, pp. 2032-6, 2010.

[14] J. A. Giesecke, M. C. Schubert, B. Michl, F. Schindler, and W. Warta, "Minority carrier lifetime imaging of silicon wafers calibrated by quasi-steady-state photoluminescence," *Solar Energy Materials and Solar Cells,* vol. 95, pp. 1011-1018, 2011.

[15] D. Macdonald, J. Tan, and T. Trupke, "Imaging interstitial iron concentrations in boron-doped crystalline silicon unsing photoluminescence," *Journal of Applied Physics,* vol. 103, pp. 073710–1–073710-7, 2008.

[16] B. Michl, M. Rüdiger, J. Giesecke, M. Hermle, W. Warta, and M. C. Schubert, "Efficiency limiting bulk recombination in multicrystalline silicon solar cells," *Solar Energy Materials & Solar Cells,* vol. 98, pp. 441-7, 2012.

[17] B. Michl, M. Kasemann, W. Warta, and M. C. Schubert, "Wafer thickness optimization for silicon solar cells of heterogeneous material quality," *Physica Status Solidi RRL – Rapid Research Letters,* vol. 7, pp. 955-8, 2013.

[18] H. Hauser, B. Michl, S. Schwarzkopf, V. Kübler, C. Müller, M. Hermle, and B. Bläsi, "Honeycomb texturing of silicon via nanoimprint lithography for solar cell applications," *IEEE Journal of Photovoltaics,* vol. 2, pp. 114-22, 2012.

[19] J. Brody, A. Rohatgi, and V. Yelundur, "Bulk resistivity optimization for low-bulk-lifetime silicon solar cells," *Progress in Photovoltaics: Research and Applications,* vol. 9, pp. 273-285, 2001.

[20] R. Einhaus, F. Duerinckx, E. Van Kerschaver, J. Szlufcik, F. Durand, P. J. Ribeyron, J. C. Duby, D. Sarti, G. Goaer, G. N. Le, I. Périchaud, L. Clerc, and S. Martinuzzi, "Hydrogen passivation of newly developed EMC-multi-crystalline silicon," *Materials Science and Engineering: B,* vol. 58, pp. 81-85, 1999.

[21] J. Schön, M. C. Schubert, H. Habenicht, and W. Warta, "2D modeling of the iron concentration from crystallization to final firing of mc silicon solar cells," in *Proceedings of the 25th European Photovoltaic Solar Energy Conference and Exhibition*, Valencia, Spain, 2010, pp. 1195-9.

[22] B. Michl, J. Schön, W. Warta, and M. C. Schubert, "The impact of different diffusion temperature profiles on iron concentrations and carrier lifetimes in multicrystalline silicon wafers," *IEEE Journal of Photovoltaics,* vol. 3, pp. 635-40, 2013.

[23] S. P. Phang and D. Macdonald, "Direct comparison of boron, phosphorus, and aluminum gettering of iron in crystalline silicon," *Journal of Applied Physics,* vol. 109, pp. 073521–1–073521-6, 2011.

[24] W. Kwapil, J. Schön, F. Schindler, W. Warta, and M. C. Schubert, "Impact of Iron Precipitates on Carrier Lifetime in As-Grown and Phosphorus-Gettered Multicrystalline Silicon Wafers in Model and Experiment," *IEEE Journal of Photovoltaics,* vol. 4, pp. 791-798, 2014.

[25] J. Haunschild, I. E. Reis, T. Chipei, M. Demant, B. Thaidigsmann, M. Linse, and S. Rein, "Rating and sorting of mc-Si as-cut wafers in solar cell production using PL imaging," *Solar Energy Materials & Solar Cells,* vol. 106, pp. 71-75, 2012.

[26] J. Schmidt, B. Lim, D. Walter, K. Bothe, S. Gatz, T. Dullweber, and P. P. Altermatt, "Impurity-related limitations of next-generation industrial silicon solar cells," *IEEE Journal of Photovoltaics,* vol. 3, pp. 114-8, 2013.

[27] J. Schön, H. Habenicht, W. Warta, and M. C. Schubert, "Chromium distribution in multicrystalline silicon: comparison of simulations and experiments," *Progress in Photovoltaics: Research and Applications,* vol. 21, pp. 676-80, 2013.